Biosensors and Bioelectronics 133 (2019) 199–204

Contents lists available at ScienceDirect

Biosensors and Bioelectronics

journal homepage: www.elsevier.com/locate/bios

Molybdenum disulfide-integrated photonic barcodes for tumor markers screening

Feika Bian[a,b], Lingyu Sun[b], Lijun Cai[b], Yu Wang[b], Yuanjin Zhao[a,b,**], Shuqi Wang[c,**], Mengtao Zhou[a,*]

[a] Pancreatitis Center, Precision Medicine Center, and Key Laboratory of Diagnosis and Treatment of Severe Hepato-Pancreatic Diseases of Zhejiang Province, The First Affiliated Hospital of Wenzhou Medical University, Wenzhou 325035, China
[b] State Key Laboratory of Bioelectronics, School of Biological Science and Medical Engineering, Southeast University, Nanjing 210096, China
[c] State Key Laboratory for Diagnosis and Treatment of Infectious Diseases, First Affiliated Hospital, College of Medicine, Zhejiang University, Hangzhou 310003, China

ARTICLE INFO

Keywords:
Molybdenum disulfide
Barcode
Colloidal crystal
Structural color
MiRNA

ABSTRACT

As a new class of two-dimensional (2D) materials, molybdenum disulfide (MoS_2) has huge potential in biomedical area; while its applications in multiplex bioassays are still a challenge. Here, we present novel MoS_2-integrated silica colloidal crystal barcode (SCCB) for multiplex microRNA (miRNA) screening. MoS_2 was adsorbed on SCCBs by electrostatic interaction, and quantum dots (QDs) decorated hairpin probes were coupled on MoS_2 by covalent linkage. As the MoS_2 could quench the QDs of the hairpin probes, they together formed a molecular beacon (MB) structure before the detection. When used in assays, target miRNA could form a double strand with the probe and made QDs keep away from MoS_2 sheets to recovery their fluorescence. Because the released QDs were positively correlated with the concentration of the hybridized nucleic acid, the target miRNAs could be quantified by measuring the fluorescence signal of the QDs on the SCCBs. In addition, by utilizing different MoS_2-integrated structural color encoded SCCBs, multiplexed miRNA quantification could also be realized. Based on this strategy, we have demonstrated that several pancreatic cancer-related miRNAs could be selectivity and sensitivity detected with a detection limit of 4.2 ± 0.3 nM. These features make the MoS_2-integrated SCCB ideal for many potential applications.

1. Introduction

Layered two-dimensional (2D) nanomaterial has important applications in biomedical sensing because of its large specific surface area and excellent optical physical, chemical and electrical properties (Anichini et al., 2018; Cai et al., 2018; Tan et al., 2017). For example, the exquisite physicochemical properties of graphene oxide (GO) lead to advantageous biosensing approaches which can improve analytical sensitivity and analysis time (Morales-Narváez and Merkoçi, 2018). Among various 2D materials, molybdenum disulfide (MoS_2), which is composed of Mo metal layers sandwiched between two sulfur layers, is becoming a popular material nowadays for its graphene-like structure and potential as biosensors and bioelectronics devices (Cheng and Wang, 2016; Cheng et al., 2018; Hirsch and Hauke, 2018; B.L. Li et al., 2017; X. Li et al., 2017; Ou et al., 2017; Wan et al., 2018; Wang et al., 2017). Due to its semiconductor ultrathin layer structure, MoS_2 exhibits photoluminescence and fluorescence quenching properties. Owing to this feature, MoS_2 has been employed for nucleic acid and protein detections (X. Li et al., 2017; B.L. Li et al., 2017; Zhu et al., 2013). Especially, the MoS_2-based sensors for microRNAs (miRNAs), which is exhibits a higher or lower expression in serum samples (200 aM to 20 pM), is expected to become an emerging highly sensitive tumor screening method (Bian et al., 2018; Labib and Berezovski, 2015; Zhu et al., 2017). However, most of the current MoS_2-based quantification methods are restricted to single target test; this is usually not sufficient to guide diagnosis, thus impeding the efficiency and practicability of miRNAs screening in clinical applications. In addition, most of the MoS_2 in these methods were fixed on planar substrates, which greatly affects the reaction rate and reaction sensitivity due to its low reaction kinetics. Thus, new MoS_2-based strategies for multiple and sensitive

* Corresponding author at: Pancreatitis Center, Precision Medicine Center, and Key Laboratory of Diagnosis and Treatment of Severe Hepato-Pancreatic Diseases of Zhejiang Province, The First Affiliated Hospital of Wenzhou Medical University, Wenzhou 325035, China.
** Corresponding authors.
E-mail addresses: bianfeika@foxmail.com (F. Bian), 1035496126@qq.com (L. Sun), 13260932100@163.com (L. Cai), 1146681561@qq.com (Y. Wang), yjzhao@seu.edu.cn (Y. Zhao), shuqi@zju.edu.cn (S. Wang), zhoumengtao@wmu.edu.cn (M. Zhou).

https://doi.org/10.1016/j.bios.2019.02.066
Received 10 January 2019; Received in revised form 26 February 2019; Accepted 27 February 2019
Available online 11 March 2019
0956-5663/

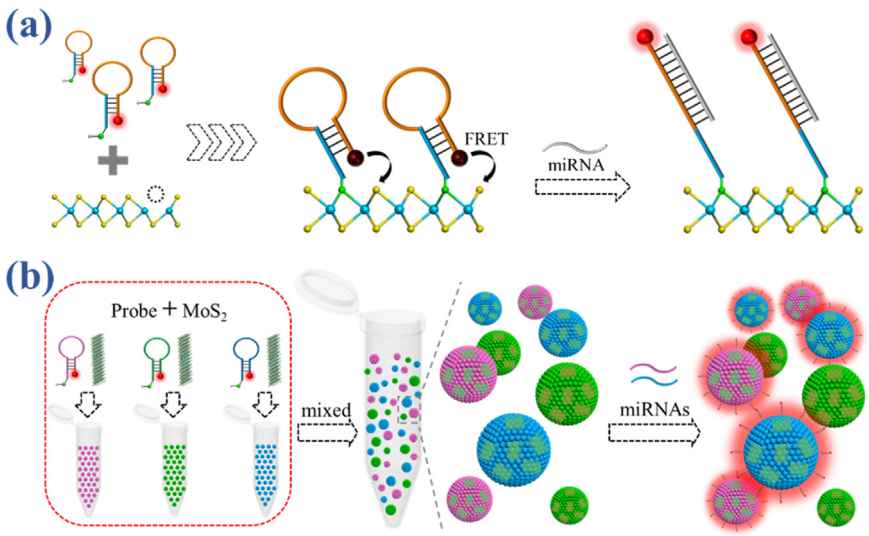

Fig. 1. (a) Schematic illustration of microRNA detection process on MoS_2 platform. **(b)** Schematic diagram of multiplex microRNA detection by MoS_2-integrated SCCBs.

miRNAs quantification are still anticipated.

Here, we reported novel MoS_2-integrated silica colloidal crystal barcodes (SCCBs) for multiplex, high-selectivity and high-sensitivity miRNAs screening, as schemed in Fig. 1. Colloidal crystals are a kind of structured materials that assembled by periodic arranged monodisperse nanoparticles, which imparts them with an advanced feature of photonic band gaps (PBGs) for light manipulation (Chen et al., 2018; Hou et al., 2018; Zhang and Khademhosseini, 2017a; Zhang et al., 2017b; Zhu et al., 2018). Owing to its brilliant optical performance, colloidal crystals have been employed as promising materials in many emerging field (Fu et al., 2017, 2018, 2018; Hou et al., 2015; Lin et al., 2017; Xu et al., 2018). Tailoring with a spherical morphology, colloidal crystal particles have also been utilized as photonic barcodes for multiple assays (Choi et al., 2018; Lee et al., 2018; Liu et al., 2018; Wang et al., 2018). Because of their PBGs encoding stability, fluorescent signal enhancement and freedom from any fluorescent background, the colloidal crystal barcodes have shown demonstrated values in many practical sample detections (Li et al., 2007a, 2007b, 2008; Xu et al., 2015; Yang et al., 2019). Nevertheless, integrating the excellent 2D material MoS_2 on the surface of the colloidal crystal barcodes for multiplex, high-selectivity and high-sensitivity miRNAs screening has never been implemented.

In this paper, we designed a quantum dots (QDs) decorated hairpin probe for label-free miRNA detection on the surface of the MoS_2-integrated SCCBs. MoS_2 was adsorbed on SCCBs by electrostatic interaction, while the hairpin probe was coupled on MoS_2 by covalent linkage (Hirsch and Hauke, 2018; Mei et al., 2018). Because the QD of the hairpin probe could be quenched by MoS_2 owing to fluorescence resonance energy transfer (FRET), they formed a molecular beacon (MB) structure (Cheng and Wang, 2016). This structure could be opened by using complementary target miRNAs, which kept QDs away from MoS_2 sheets to recover the fluorescence of QDs (Fig. 1**a**). Thus, the target miRNAs could be quantified by measuring the fluorescent signal of QDs which was positively correlated with their concentration. In addition, by utilizing different MoS_2-integrated SCCBs, multiplexed miRNA quantification could be realized. Based on this strategy, we have demonstrated that several pancreatic cancer-related miRNAs could be detected in a single assay (Fig. 1**b**). These results indicate that the MoS_2-integrated SCCBs are of great value in human tumor markers screening.

2. Experimental methods

2.1. Materials

3-Aminopropyltriethoxysilane (APTES, 98%) and 4-Morpholineethanesulfonic acid hydrate (MES) were obtained from Sigma-Aldrich (Shanghai, China). Molybdenum disulfide (MoS_2) solution (2 mg ml^{-1}) was purchased from Nanjing XF Nano Material Tech Co., Ltd. (Nanjing, China). Oligonucleotides (Table S1) were synthesized by Sangon Biotech Co., Ltd. (Shanghai, China). Carboxyl-modified semiconductor quantum dots (CdSe/ZnS) were brought from Xingzi new material technology development Co., Ltd. (Shanghai, China). Ethanol, ammonium hydroxide, 1-ethyl-3-(3-dimethylaminopropyl) carbodiimide (EDC) and tetraethylorthosilicate (TEOS) were purchased from Aladdin Reagent Co., Ltd., (Shanghai, China). Milli-Q (Millipore, Bedford, MA) water with ultraviolet sterilization was used throughout the experiment. All the chemical reagents were of the best grade available and used as received.

2.2. Preparation of silica nanoparticles

Silica nanoparticles were synthesized by the Stöber method. TEOS was added dropwise into the mixture of ethanol (300 ml) and ammonium hydroxide (10 ml). Through the hydrolysis and condensation reactions of TEOS, silica nanoparticles grow continuously in 30 °C with stirring (300 rpm). Sampling every half hour to get the desired particle size.

2.3. Preparation of SCCBs

The microfluidic droplet device was used to generate the SCCBs using the assembly of silica nanoparticles by method according to our previous work (Zhao et al., 2008). The syringe pumps and constant pressure pumps were purchased from Longer Precision Pump Co., Ltd. The continuous phase in this protocol was silicone oil (Shinetsu, 50cs, Japan) and the dispersed phase was the monodisperse silica nanoparticles aqueous suspension. The silica nanoparticle aqueous suspension was cut into droplets by silicone oil in the microfluidic droplet device. Then the droplets were evaporated at 80 °C for 8 h to achieve the colloidal crystal beads. After that we used hexane to remove the silicone oil on the beads several times. At last, the SCCBs should be calcined to stabilize the structure at 800 °C for 12 h in a muffle furnace.

2.4. Preparation of MoS_2-integrated SCCBs

After calcining, the SCCBs were dispersed in ethyl alcohol (5 ml) with 2 v/v % APTES (100 μl) and then shook at room temperature (25 °C) for 6 h (Thermomixer comfort 5355, Eppendorf, Germany). After the reaction finished, the positively charged aminated SCCBs were carefully washed with ethyl alcohol several times to remove redundant APTES. In order to make the MoS_2 evenly distributed on the SCCBs, MoS_2 solution (2 mg ml^{-1}) was shocked with ultrasound for 1 h before usage at room temperature (25 °C). Then, 100 μl MoS_2 (2 mg ml^{-1}) was mixed with aminated SCCBs in DI water at room temperature (25 °C) for 2 h. After that, the MoS_2-integrated SCCBs were washed with DI water for several times to remove unfixed MoS_2.

2.5. MicroRNA detection based on MB

The amino modified probe sequences (10 μM, 2 μl) were incubated with the carboxyl modified quantum dots (5 μM, 1 μl) in 1 ml MES solution (pH 6.0) at room temperature (25 °C) for 1 h. Then, the freshly prepared 1 μl EDC stock solution (10 mg EDC with 1 ml MES) was added to the solution. The mixture was incubated for 3 h under continuous stirring at room temperature (25 °C). Then, the QD-decorated probes were separated by ultrafiltration tube (12,000 rpm), and these thiol-modified QD-probes were incubated with MoS_2-integrated SCCBs for 2 h and then were washed with DI water for several times to remove dissociative probe. Finally, the MoS_2-integrated SCCBs were used for miRNA quantification. The solution containing target miRNAs (different concentration) was used to incubate the SCCBs. After then, SCCBs were washed by DI water to remove redundant target.

2.6. Multiplex microRNAs quantification

Three kinds of MoS_2-integrated SCCBs were mixed with excessive probes (2×10^{-7} M) in DI water for 2 h at 25 °C in the constant shaker, respectively. Various combinations of three targets (miR-155, miR-181a, miR-210) were added into the solutions and incubated for 2 h. Finally, the SCCBs were washed three times with DI water.

2.7. Characterization

A field emission scanning electron microscope (FESEM, Zeiss, Ultra Plus, Resolution: 1 nm@15 kV) and a transmission electron microscope (TEM, jeol, JEM-2100, Lattice Resolution: 0.14 nm, Point Resolution:0.23 nm, Accuracy of Magnification: ± 10%) were used to characterize the microstructures of the MoS_2-integrated SCCBs and QD-probe decorated MoS_2. Optical images of three kinds of SCCBs were snapped by the stereoscopic microscope (Jiang Nan) equipped with CCD camera (Olympus, DP30BW). The reflectance spectra of the barcodes were detected and recorded by the same microscope equipped with a fiber optic spectrometer (Ocean Optics, USB 2000 +, wavelength coverage: 200–1025 nm, integral time: 1 ms-65 s (20 s typical), optical resolution: 1.7–2.1 nm FWHM). Cross-section fluorescence images of the barcodes were snapped by a laser scanning confocal microscope (Carl Zeiss, LSM510). The fluorescence intensity was measured by a fluorescence microscope (Olympus, CKX41) equipped with the same optic spectrometer. And the fluorescence images of multiplex detection were snapped by the same fluorescence microscope.

3. Results and discussion

3.1. Design of the MoS_2-integrated SCCBs

In a typical experiment, silica nanoparticles were self-assembled in microfluidic droplets to fabricate the silica colloidal crystal particles. Owing to the abundant silanol groups (Si-OH) on the surface of silica nanoparticles, the colloidal crystal could bind with desired functional groups after simple modification for immobilization of biomolecules. A positively charged aminated silica colloidal crystal particles could be obtained by modified with 3-Aminopropyltriethoxysilane (APTES). Subsequently, MoS_2 nanosheets were added in the DI water with aminated silica colloidal crystal particles. Because MoS_2 was negatively charged, it could adhere to the surface of aminated colloidal crystal tightly through electrostatic interactions. Noted that, the periodic ordered nanostructure of the silica colloidal crystal barcodes (SCCBs) would not be interfered since the integration of MoS_2 and subsequent bio-detection only occurred on the surface of the colloidal crystal. Therefore, the MoS_2-integrated SCCBs were also imparted with photonic bandgap (PBG) properties, which endow the barcodes with glamorous structural colors and distinguishable reflection peaks. Generally, the characteristic reflection peak position of SCCBs which consist of different diameter silica nanoparticles could be calculated by Bragg's equation (Park and Xia, 1999; Gu et al., 2001),

$$\lambda = 1.633 d n_{average}$$

where λ is on behalf of the peak wavelength of the barcode, d refers to the diameter of the uniform silica nanoparticles which constitute SCCBs, and the average refractive index is represented by $n_{average}$. Therefore, the peak value λ is only affected by the different size of the silica nanoparticles under constant external conditions. It means that the SCCBs with different reflection peaks can be obtained by changing different silica nanoparticles. The optical images showed the MoS_2-integrated SCCBs were brilliant and they had distinct reflection peaks (Fig. 2**a–d**). Theoretically, the SCCBs could be clearly distinguished when the interval between the different reflection peaks is more than 20 nm. Thus, there are about 21 kinds of barcodes could be employed for subsequent bio-detection over the visible range of 380–780 nm without code interference, simultaneously. In order to investigate the microstructure of the MoS_2-integrated SCCBs, scanning electron microscopy (SEM) was used to characterize them. As shown in Fig. 2**e**, after amination modification, the silica nanoparticles were still closely packed and formed an ordered hexagonal alignment. Owing to the electrostatic adsorption, MoS_2 could adhere on the surface of amination modified SCCBs (Fig. 2**f**). These results indicated that the MoS_2-integrated SCCBs had stable coding and could be used to couple with miRNAs probe for multiplexed detection.

3.2. Optimization of reaction conditions

Despite exhibiting similar morphology with graphene, nucleic acid-modified methods of MoS_2 were thiols substituted sulfur atoms or healing the defects of MoS_2 sheets by thiols, instead of π–π stacking interaction. Compared with the weak van der Waals forces between the DNA sequences and MoS_2 sheets, covalent connection was a more effective and robust way of bio-modification. To investigate the reaction mechanism of MoS_2-based miRNAs detection, 5′-end thiol-modified labels were chosen to construct the detection platform. Sulfhydryl decorated ssDNA and hydroxyl decorated ssDNA were incubated with MoS_2 sheets, respectively. All of the probes were linked with QDs on the 3′-end of the sequences. Transmission electron microscopy (TEM) images showed the difference between these two kinds of labels (Fig. S1). Owing to the thiols, sulfhydryl decorated label could covalently connect to MoS_2 sheets. However, few hydroxyls decorated labels could adhere on MoS_2 by van der Waals forces. MoS_2-integrated SCCBs were also used to explore appropriate connection methods. Confocal laser scanning microscopy (CLSM) images showed the same result (Fig. S2). The signal could only be found on the surface of SCCBs which incubated with thiol-modified labels, while hydroxyl decorated ssDNA could not adhere on MoS_2-integrated SCCBs. In order to calculate the amount of probes on the surface of the barcodes, the photoluminescence (PL) intensity of QD-decorated probes was measured to indirectly embody the quantity. The standard curve represented the fluorescence intensity corresponding to the QD-decorated probes of known concentration (Fig.

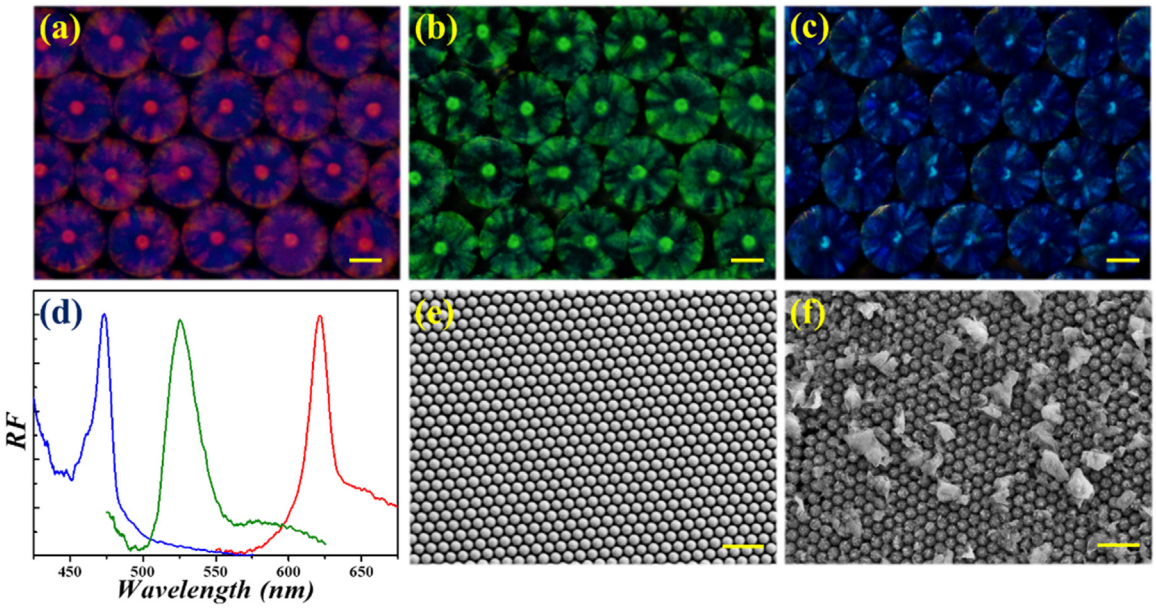

Fig. 2. (a-c) Reflection images of three kinds of SCCBs. Scale bar is 200 μm. **(d)** Reflection spectra of these three kinds of SCCBs. **(e-f)** SEM images of **(e)** the surface of amination modified SCCBs; **(f)** the surface of MoS_2-integrated SCCBs. Scale bar is 800 nm.

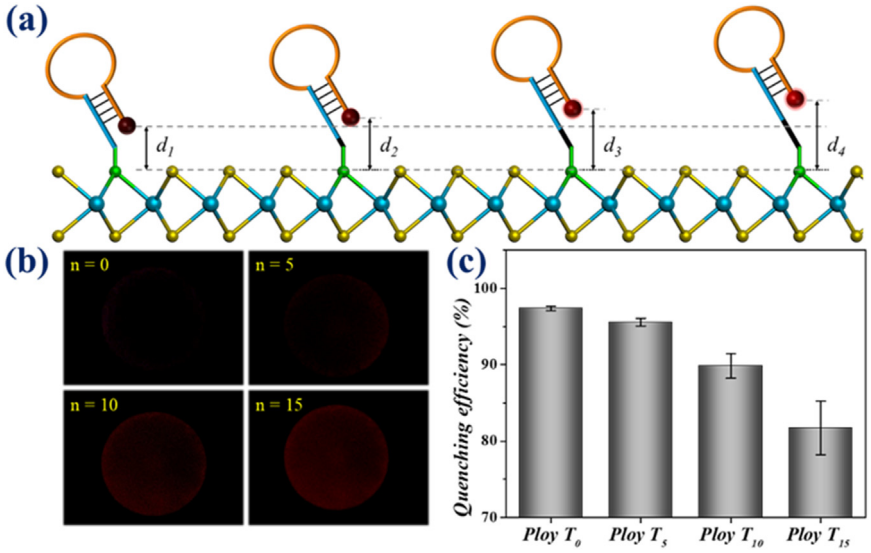

Fig. 3. (a) Schematic illustration of Poly T_n probe with different lengths of QD-decorated probe anchored on MoS_2 (n = 0, 5, 10, 15, respectively). **(b)** Fluorescence images of different poly T_n probe. **(c)** The quenching efficiency statistics of different poly T_n probe.

S3a). By subtracting the fluorescence intensity value of the probe solution before and after the reaction, the number of QD-decorated probes coupled to each barcodes could be obtained (Fig. S3b). After calculation, there were about 3×10^{12} probes on each SCCB. Considering the high fluorescence quenching properties of MoS_2 sheets as a semiconductor, we explored the quenching efficiency by adjusting the poly T length. Poly T_n is a sequence consisted of continuous T basic group and n represents the number of T basic group. As the poly T_n sequence increased, the distance between the QD and MoS_2 integrated on the SCCB was getting farther, and the quenching effect was gradually weakened (Fig. 3**a**). Fluorescence images showed the intensity of the QD-decorated probes on MoS_2-integrated SCCBs increased (i.e., lower quenching efficiency) with the increase of poly T length (Fig. 3**b**). Afterwards, the fluorescence intensity of different kinds of barcodes were measured and counted. The quenching efficiencies of different length probes were 97.4%, 95.6%, 89.8% and 81.7% (Fig. 3**c**). These results showed that the quenching effect was inversely proportional to the distance between QD and MoS_2 sheets. Therefore, shortest probes without poly T were used in subsequent experiments.

3.3. Detection performance of the MoS_2-integrated SCCBs

The QD-decorated probe and the MoS_2 sheets modified on SCCBs formed a MB (molecules beacon) structure together. Without target, QD was close enough to MoS_2 sheets, and the fluorescence of QD could be absorbed by MoS_2. Thus the fluorescence was almost quenched and the fluorescence background was extremely weak. Matched miRNAs could open the MB by complementary base pairing, and the QDs could keep away from MoS_2 sheets. After hybridization, the fluorescence of QD recovered almost 100%. Therefore, this strategy could be utilized for miRNA quantification by detecting the fluorescent intensity of QDs which was positively correlated with target miRNA concentration. The fluorescence spectrum of each barcode was measured by a spectrometer attached to the microscope. With the increasing concentration of target

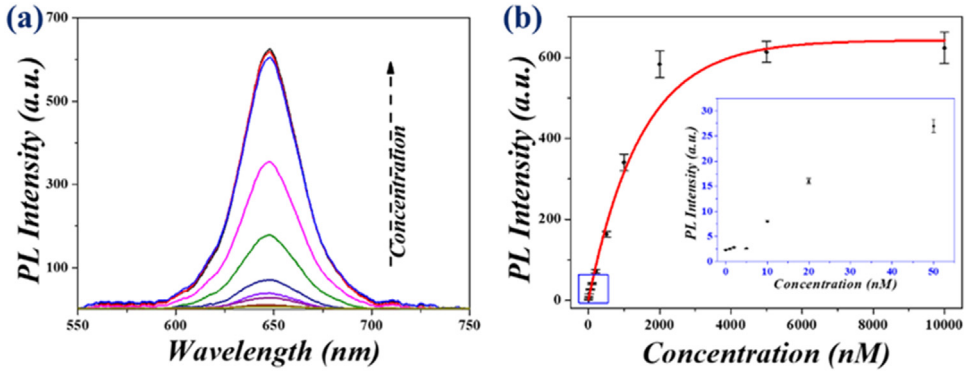

Fig. 4. (a) The fluorescence spectrum of MoS_2-integrated SCCBs after incubation with different concentration of target miRNA. **(b)** The relationship of the fluorescence intensity with target miRNA concentration in DI water. The limit of detection was 4.2 ± 0.3 nM and the linear detection range was 10 nM to 2 μM.

miRNA for opening the hairpin probe in DI water, the fluorescence emission intensity of QDs increased (Fig. 4**a**). The relationship of the fluorescence intensity versus the value of miRNA concentration showed a linear calibration in the range from 10 to 2000 nM (Fig. 4**b**). And the fluorescence signal reached a maximum when the target concentration reached 2 μM. The spectrum indicated that fluorescence signal could be detected obviously when the concentration reached 10 nM for miRNA (inset of Fig. 4**b**). As shown in Fig. S5, according to the formula of 3STD, when the target concentration is as low as 4.2 ± 0.3 nM, it could be detected with high sensitivity. By taking the values into the standard curve in Fig. S3a, it could be calculated that there were about 2×10^{12} hairpin structures of QD-decorated probe opened by target miRNA on each barcode (there were about 3×10^{12} probes on each SCCB). Thus, the hybridization efficiency of hairpin probes and target miRNAs was about 66% in our assay protocol, not all probes are hybridized with the target. These results suggested that the MoS_2-integrated SCCBs were appropriate for quantification of miRNA.

3.4. Tumor marker detection by MoS_2-integrated SCCBs

Pancreatic cancer is a malignant tumor of the digestive tract with a high incidence and mortality. Compared with normal tissues, miRNA-155, miRNA-181a and miRNA-210 were found to exhibit high expression in pancreatic cancer. Thus, multiplex detection of these miRNAs has extremely important application prospects. To demonstrate the multiplex detection performance of the MoS_2-integrated SCCBs as encoded micro-carriers in clinical analysis, three kinds of SCCBs with characteristic reflection peaks at 473 nm (blue), 525 nm (green) and 621 nm (red) were chosen to capture miRNAs, simultaneously (Fig. 1**b**). Each kind of MoS_2-integrated SCCBs was assembled with unique probe, respectively. Then three kinds of miRNAs were incubated with the mixed barcodes which could capture corresponding miRNA target and open the hairpin in DI water. After hybridization process, the microscope images showed that fluorescence signals of QD-decorated probes were only observed on the barcodes with target miRNA existence (Fig. S4**a-f**). The histogram was a statistic of fluorescence on different SCCBs for intuitive expression of the selectivity (Fig. S4g). To further verify the performance of the MoS_2-integrated SCCBs for detection in mixed samples, the three barcodes were incubated with two or three kinds of target miRNAs. As shown in Fig. 5, blue barcodes coupled the QD-decorated probe for miR-155, green barcodes were ready for detecting miR-181a and the probe on red barcode could capture miR-210. When the mixed sample contained miR-155 and miR-181a, the fluorescence signal of QDs could be found on blue barcodes and green barcodes (Fig. 5**a** and **e**). The combination of several other samples exhibited the same result (Fig. 5**b-d** and **f-i**). These results indicated that the MoS_2-integrated SCCBs could analyze different miRNAs of pancreatic cancer samples without interference among several kinds of targets (Fig. 5**j**). Therefore, the MoS_2-integrated SCCBs are a potential technology for tumor miRNA screening and other practical applications.

4. Conclusion

In this work, we have developed a novel MoS_2-integrated SCCBs for tumor miRNAs quantification. High sensitivity and selectivity detection could be realized by measuring the fluorescent signal of the QDs which was positively correlated with the concentration of miRNAs. This strategy has achieved the detection of pancreatic cancer-associated miRNAs with a detection limit of 4.2 ± 0.3 nM and the linear detection range was 10 nM to 2 μM. In addition, several miRNAs could be analyzed simultaneously by using different SCCBs with stable encoding. We anticipate that the MoS_2-integrated SCCBs provide new opportunities for a wide range of practical applications.

Acknowledgements

This work was supported by the National Key Research and Development Program of China (2017YFA0700404, 2016YFC1101302), the National Natural Science Foundation of China (Grants 51522302, 21473029, 61827806 and 31871016), the NSAF Foundation of China (grant U1530260), the Natural Science Foundation of Jiangsu Province (Grant no. BE2018707), the National Science and Technology Major Project (2018ZX10732401-003-007), the Fundamental Research Funds for the Central Universities, and the Scientific Research Foundation of Southeast University.

Author contributions

Y.J.Z. conceived the conceptualization and designed the experiment; F.K.B. carried out the experiments, did the investigation and validation; F.K.B., L.Y.S. and Y.J.Z. curated the data and wrote the original draft; L.Y.S., L.J.C., Y. W., K.Q.S., M.T.Z. and S.Q.W. contributed to scientific discussion of the article and writing - review & editing.

Notes

The authors declare no competing financial interest.

Declaration of interest statement

We declare that we do not have any commercial or associative interest that represents a conflict of interest in connection with the work submitted.

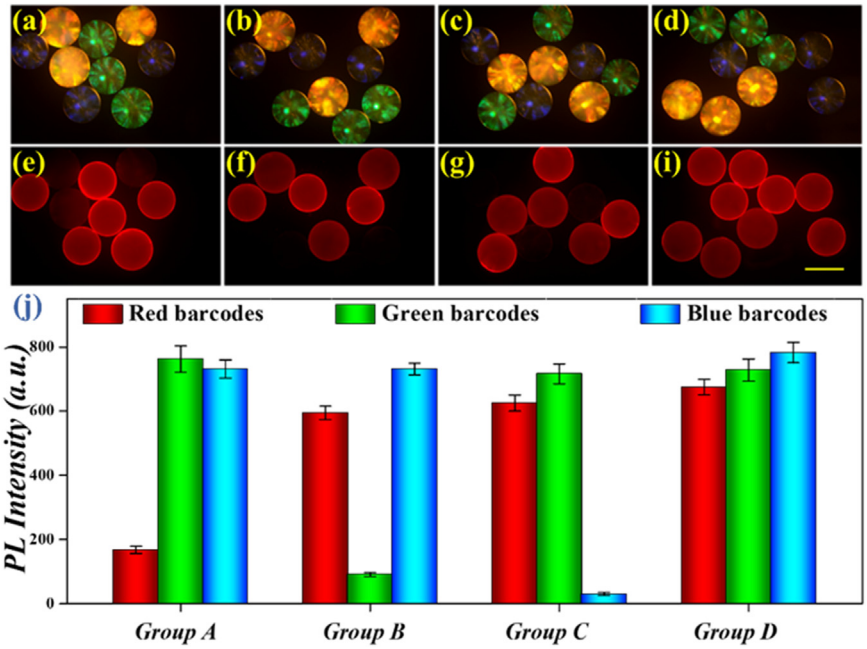

Fig. 5. Bright field images **(a-d)** and fluorescence images **(e-i)** of three kinds of MoS_2-integrated SCCBs after incubating with target miRNA; Scale bar is 300 μm. **(j)** The fluorescence statistics after incubating three different MoS_2-integrated SCCBs with different combination of targets. Group A contained miR-181a, miR-155; Group B contained miR-210, miR-155; Group C contained miR-210, miR-181a; Group D contained all of three target.

Appendix A. Supporting information

Supplementary data associated with this article can be found in the online version at https://doi.org/10.1016/j.bios.2019.02.066.

References

Anichini, C., Czepa, W., Pakulski, D., Aliprandi, A., Ciesielski, A., Samorı`, P., 2018. Chem. Soc. Rev. 47, 4860–4908.

Bian, F.K., Wu, J.D., Wang, H., Sun, L.Y., Shao, C.M., Wang, Y., Li, Z.Y., Wang, X.H., Zhao, Y.J., 2018. Small 14, 1803551.

Cai, X.K., Luo, Y.T., Liu, B.L., Cheng, H.M., 2018. Chem. Soc. Rev. 47, 6224–6266.

Chen, Z.Y., Fu, F.F., Yu, Y.R., Shang, Y.X., Wang, H., Zhao, Y.J., 2018. Adv. Mater. 31, 1805431.

Cheng, C.L., Wang, D.Y., 2016. Angew. Chem. Int. Ed. 55, 6853–6857.

Cheng, C.L., Cai, Y.Q., Guan, G.J., Yeo, L., Wang, D.Y., 2018. Angew. Chem. Int. Ed. 57, 11177–11181.

Choi, T.M., Je, K., Park, J.G., Lee, G.H., Kim, S.H., 2018. Adv. Mater. 30, 1803387.

Fu, F.F., Chen, Z.Y., Zhao, Z., Wang, H., Shang, L.R., Gu, Z.Z., Zhao, Y.J., 2017. Proc. Natl. Acad. Sci. USA 114, 5900–5905.

Fu, F.F., Shang, L.R., Chen, Z.Y., Yu, Y.R., Zhao, Y.J., 2018. Sci. Robot. 3, eaar8580.

Fu, Q.Q., Zhu, H.M., Ge, J.P., 2018. Adv. Funct. Mater. 28, 1804628.

Gu, Z.Z., Kubi, S., Qian, W.P., Einaga, Y., Tryk, D.A., Fujishima, A., Sato, O., 2001. Langmuir 17, 6751–6753.

Hirsch, A., Hauke, F., 2018. Angew. Chem. Int. Ed. 57, 4338–4354.

Hou, J., Li, M.Z., Song, Y.L., 2018. Angew. Chem. Int. Ed. 57, 2544–2553.

Hou, J., Zhang, H.C., Yang, Q., Li, M.Z., Jiang, L., Song, Y.L., 2015. Small 11, 2738–2742.

Labib, M., Berezovski, M.V., 2015. Biosens. Bioelectron. 68, 83–94.

Lee, S.S., Kim, J.B., Kim, Y.H., Kim, S.H., 2018. Sci. Adv. 4, eaat8276.

Li, B.L., Setyawati, M.I., Chen, L.Y., Xie, J.P., Ariga, K., Lim, C.T., Garaj, S., Leong, D.T., 2017. ACS Appl. Mater. Interfaces 9, 15286–15296.

Li, M.Z., Liao, Q., Zhang, J.P., Jiang, L., Song, Y.L., Zhu, D.B., Chen, D., Tang, F.Q., Wang, X.H., 2007a. Appl. Phys. Lett. 91.

Li, M.Z., Xia, A.D., Wang, J.X., Song, Y.L., Jiang, L., 2007b. Chem. Phys. Lett. 444, 287.

Li, M.Z., He, F., Liao, Q., Liu, J., Liang, X., Jiang, L., Song, Y.L., Wang, S., Zhu, D.B., 2008. Angew. Chem. 120, 7368–7372.

Li, X., Shan, J.Y., Zhang, W.Z., Su, S., Yuwen, L.H., Wang, L.H., 2017. Small 13, 1602660.

Lin, C.X., Jiang, Y., Tao, C.A., Yin, X.P., Lan, Y., Wang, C., Wang, S.Q., Liu, X.Y., Li, G.T., 2017. ACS Appl. Mater. Interfaces 9, 11770–11779.

Liu, Y.X., Shang, L.R., Wang, H., Zhang, H., Zou, M.H., Zhao, Y.J., 2018. Mater. Horiz. 5, 979–983.

Mei, J.C., Li, Y.T., Zhang, H., Xiao, M.M., Ning, Y., Zhang, Z.Y., Zhang, G.J., 2018. Biosens. Bioelectron. 110, 71–77.

Morales-Narváez, E., Merkoçi, A., 2018. Adv. Mater. 31, 1805043.

Ou, X.W., Hong, F., Zhang, Z.Y., Cheng, Y., Zhao, Z.J., Gao, P.C., Lou, X.D., Xia, F., Wang, S.T., 2017. Biosens. Bioelectron. 89, 417–421.

Park, S.H., Xia, Y., 1999. Langmuir 15, 266–273.

Tan, C.L., Cao, X.H., Wu, X.J., He, Q.Y., Yang, J., Zhang, X., Chen, J.Z., Zhao, W., Han, S.K., Nam, G.H., Sindoro, M., Zhang, H., 2017. Chem. Rev. 117, 6225–6331.

Wan, S.J., Fang, S.L., Jiang, L., Cheng, Q.F., Baughman, R.H., 2018. Adv. Mater. 30, 1802733.

Wang, H., Zhao, Z., Liu, Y.X., Shao, C.M., Bian, F.K., Zhao, Y.J., 2018. Sci. Adv. 4, eaat2816.

Wang, J., Sun, L.Y., Zou, M.H., Gao, W., Liu, C.H., Shang, L.R., Gu, Z.Z., Zhao, Y.J., 2017. Sci. Adv. 3, e1700004.

Xu, L.P., Chen, Y.X., Yang, G., Shi, W.X., Dai, B., Li, G.N., Cao, Y.H., Wen, Y.Q., Zhang, X.J., Wang, S.T., 2015. Adv. Mater. 27, 6878–6884.

Xu, W.J., Li, Z.W., Yin, Y.D., 2018. Small 14, 1801083.

Yang, M.Z., Liu, Y., Jiang, X.Y., 2019. Chem. Soc. Rev. https://doi.org/10.1039/C8CS00303C.

Zhang, Y.S., Khademhosseini, A., 2017a. Science 356, eaaf3627.

Zhang, Y.S., Zhu, C.L., Xia, Y.N., 2017b. Adv. Mater. 29, 1701115.

Zhao, Y.J., Zhao, X.W., Sun, C., Li, J., Zhu, R., Gu, Z.Z., 2008. Anal. Chem. 80, 1598–1605.

Zhu, B.T., Fu, Q.Q., Chen, K., Ge, J.P., 2018. Angew. Chem. 130, 258–262.

Zhu, C.F., Zeng, Z.Y., Li, H., Li, F., Fan, C.H., Zhang, H., 2013. J. Am. Chem. Soc. 135, 5998–6001.

Zhu, D., Liu, W., Zhao, D.X., Hao, Q., Li, J., Huang, J.X., Shi, J.Y., Chao, J., Su, S., Wang, L.H., 2017. ACS Appl. Mater. Interfaces 9, 35597–35603.